Silicon and III-V compound nanotubes: Structural and electronic properties

E. Durgun, S. Tongay, and S. Ciraci*
Department of Physics, Bilkent University, Ankara 06800, Turkey
(Received 22 October 2004; revised manuscript received 27 April 2005; published 12 August 2005)

Unusual physical properties of single-wall carbon nanotubes have started a search for similar tubular structures of other elements. In this paper, we present a theoretical analysis of single-wall nanotubes of silicon and group-III-V compounds. Starting from precursor graphenelike structures we investigated the stability, energetics, and electronic structure of zigzag and armchair tubes using the first-principles pseudopotential plane wave method and finite temperature *ab initio* molecular dynamics calculations. We showed that $(n,0)$ zigzag and (n,n) armchair nanotubes of silicon having $n \geqslant 6$ are stable but those with $n<6$ can be stabilized by internal or external adsorption of transition metal elements. Some of these tubes have a magnetic ground state leading to spintronic properties. We also examined the stability of nanotubes under radial and axial deformation. Owing to the weakness of radial restoring force, stable Si nanotubes are radially soft. Undeformed zigzag nanotubes are found to be metallic for $6 \leqslant n \leqslant 11$ due to the curvature effect; but a gap starts to open for $n \geqslant 12$. Furthermore, we identified stable tubular structures formed by the stacking of Si polygons. We found AlP, GaAs, and GaN (8,0) single-wall nanotubes stable and semiconducting. Our results are compared with those of single-wall carbon nanotubes.

DOI: 10.1103/PhysRevB.72.075420 PACS number(s): 73.22.−f, 68.43.Bc, 73.20.Hb, 68.43.Fg

I. INTRODUCTION

Carbon nanotubes are unique one-dimensional nanostructures[1] with their exceptional mechanical, electronic, and magnetic properties.[2–5] While the use of single-wall carbon nanotubes (SWCNTs) requires a completely different paradigm in the development of nanodevices, Si still continues to attract interest for electronic applications in nanotechnology. Therefore, Si-based nanotubes have been the subject of experimental and theoretical analysis.

Even if a single-wall Si nanotube (SWSiNT) has never been observed, theoretical predictions have been performed for various kinds of Si tubes. Fagan *et al.*[6,7] have investigated the structural and electronic properties of chiral SWSiNTs based on density functional theory (DFT). Barnard and Russo[8] have examined the dependence of the heat of formation and the binding energy of SWSiNTs on their radius and chirality. The stability of (10,0) SWSiNT has been examined by using the empirical Monte Carlo molecular dynamics method and found that it is stable at finite temperature.[7] Ivanovskaya *et al.*[9] investigated hypothetical Si nanotubes containing regular chains of metallocarbonedrenes using a one-dimensional tight-binding model within the Hückel approximation. By using *ab initio* calculations, Dumitrica *et al.*[10] described how the smallest (2,2) and (3,0) SiNTs are stabilized by the axially placed metal atoms from different groups of the Periodic Table. Ponomarenko *et al.*[11] studied the energetics and relative stability of infinite and finite, clean, and hydrogenated open-ended Si nanotubes by using the extended Brenner potential. The existence of H-doped stable tube-shaped finite SiNTs have been predicted[12] and their electronic structures have been compared with those of carbon nanotubes.[13] Seifert *et al.*[14] have argued that structures of silicate and SiH nanotubes are more stable than bare Si nanotubes. Singh *et al.*[15] have investigated the stability of finite and infinite hexagonal prismatic structures of Si with 3*d* magnetic elements and predicted that such structures can be stabilized through doping by the transition metal (TM) elements. Fullerene-structured Si tubulars, possibly based on Si_{24} have been produced.[16] More recently, the successful synthesis of multiwalled Si nanotubes has been reported.[17] Now, SWSiNTs are no longer hypothetical structures and it is not unrealistic to expect their fabrication with controllable size and diameter. Similarly, achievements of the synthesis of single-wall BN nanotubes[18] and GaN (Refs. 19 and 20) and AlN (Ref. 21) thick-wall tubular forms has increased the interest in the theoretical analysis of compound nanotubes.[22–25] In addition, the synthesis of Mo and W chalcogenide nanotubes[26–28] and also NiCl tubular and cage structures have been realized.[29]

In this paper we present a theoretical analysis of Si nanotubes and III-V compound nanotubes based on state-of-the-art first-principles calculations. Our work is concentrated mainly on the tube structures which can be viewed as the rolling of graphenelike honeycomb planes of Si or III-V elements on a cylinder of radius *R*. Starting from the precursor graphenelike honeycomb structures we investigated their stability, energetics, and electronic properties of these nanotubes. Since O, O_2, Si, Au, and H are critical elements for various processes on Si, we also examined the adsorption of these atoms on SWSiNT. Finally, we studied the stabilization of unstable, small-diameter SWSiNTs through the internal and external adsorption of transition metal elements. In addition, we found that tubular structures which are generated by stacking of triangles, pentagons, and hexagons of Si are stable and metallic. The (8,0) zigzag tubes of AlP, GaN, and GaAs are stable and semiconducting. The results obtained from the present study have been compared systematically with those of SWCNT. The stable tube structures predicted in this study are hoped to motivate experimental research aiming at the synthesis of various tubular structures of group-IV elements and III-V and II-VI compounds.

II. METHOD

We have performed first-principles plane wave calculations[30,31] within DFT[32] using ultrasoft pseudopotentials.[31,33] The exchange correlation potential has been approximated by the generalized gradient approximation (GGA).[34] Structures incorporating TM atoms have been calculated using spin-polarized GGA. For partial occupancies we use the Methfessel-Paxton smearing method.[35] The width of smearing is chosen between 0.01–0.1 eV, depending on the system. All structures have been treated by supercell geometry using the periodic boundary conditions. To prevent interactions between adjacent structures, a large spacing (~10 Å) has been taken. Convergence with respect to the number of plane waves used in expanding Bloch functions and **k** points in sampling the Brillouin zone are tested for the parent bulk crystals as well as tubular structures. In the self-consistent potential and total energy calculations, the Brillouin zone of nanotubes has been sampled by $(1\times1\times19)$ mesh points in **k** space within the Monkhorst-Pack scheme.[36] Calculations of graphene and graphite structures have been carried out using $(19\times19\times1)$ and $(8\times8\times6)$ **k** point samplings, respectively. A plane-wave basis set with kinetic energy cutoff 200 eV $\leqslant \hbar^2|\mathbf{k}+\mathbf{G}|^2/2m \leqslant$ 330 eV has been used. All atomic positions and lattice parameters are optimized by using the conjugate gradient method where total energy and atomic forces are minimized. The convergence for energy is chosen as 10^{-5} eV between two ionic steps, and the maximum force allowed on each atom is 0.05 eV/Å.

It should be noted that DFT-based methods provide reliable predictions, for the ground state properties, but band gaps are usually underestimated. Hence the energy band structure obtained from the single-particle energy eigenvalues of Kohn-Sham equations are only approximations to the real energy bands. Proper many-body self-energy corrections can be made by using the *GW* method.[37] Recently, *GW* energies are compared with DFT local-density-approximation (LDA) results of $(n,0)$ SWCNTs, which indicate shifts of valence and conduction bands and a considerable increase of the LDA band gap from 0.2 eV to 0.6 eV.[38] It is suggested that *GW* corrections are small for large radius SWCNTs. Performing first-principles many-body Green's function calculations Spataru *et al.*[39] showed that the optical spectrum of both semiconducting and metallic small-radius SWCNTs exhibit important excitonic effects due to quasi-one-dimensional nature. It is interesting to note that while the band gaps of (9,0), (12,0), and (15,0) zigzag SWCNTs have been measured by scanning tunneling spectroscopy[40] to be 80, 42, and 29 meV, respectively, the same band gaps have been predicted by GGA calculations[41] to be 93, 78, and 28 meV, respectively.

The stability of the structures we studied is the most crucial aspect of our work, since it provides valuable information for the synthesis of these materials in the future. In this respect an extensive analysis of stability has been carried out for various nanotubes. First, we applied a radial deformation to certain nanotubes and optimized their structures to see whether they relax to their original, undeformed circular forms under zero external force. Furthermore, we have performed, finite-temperature *ab initio* molecular dynamics calculations up to 1000 K using the Nosé thermostat[42] for 250 time steps (0.5 ps) to check whether the optimized structure will be affected from random thermal motion of atoms or whether they maintain their tubular form at high temperatures. We believe that if there were any kind of structural instability, it would be initiated and also enhanced within these time steps at high temperatures.

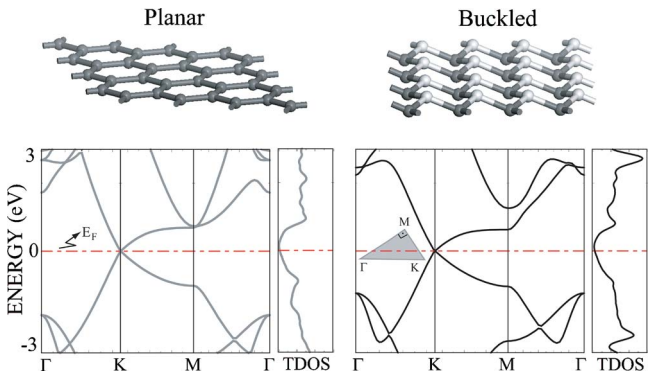

FIG. 1. (Color online) Band structure and TDOS analysis for planar and HC of Si. Light lines correspond to planar (having $P6/MMM$ symmetry) and dark lines correspond to buckled structure (having $P\text{-}3M1$ symmetry). The zero of energy is set to the Fermi level E_F. The inset shows the 1/12 of hexagonal Brillouin zone.

III. HONEYCOMB STRUCTURE OF SILICON AND III-V COMPOUNDS

One of the main difficulties for synthesizing Si nanotubes seems to be the absence of a two-dimensional (2D) silicon layer similar to the graphene structure of carbon. This is traced to the fact that in contrast to carbon, sp^3 hybridization in Si is more stable than sp^2 hybridization.[43] In view of this situation, we examined whether the graphenelike 2D sheet of silicon can be stable. Two-dimensional hexagonal lattice forming a honeycomb structure in the *xy* plane has been periodically repeated along the *z* axis with 10 Å spacing to minimize interlayer interactions. In order to reduce the effects of the constraints to be imposed by using the primitive unit cell, we performed structure optimizations on the (2×2) cell in the *xy* plane. Our calculations revealed that the planar structure (where all atoms lie in the same plane) is metastable, but it is buckled by a 0.45 Å relative vertical displacement of alternate atoms on the hexagons. The gain of energy upon buckling is 30 meV/atom. The binding energy is calculated to be 4.9 eV/atom which is 0.6 eV lower than the Si diamond structure and the average distance between nearest Si atoms is 2.2 Å. In the rest of the paper, this graphenelike structure will be specified as the buckled honeycomb structure. As shown in Fig. 1, the detailed band structure and total density of states (TDOS) analysis indicate that both buckled and planar systems have large band gaps along ΓK and MK directions, but conduction and valence bands cross the Fermi level at the **k** point of the Brillouin

zone. The electronic structure of the system does not change significantly as a result of buckling, except some of the bands split due to the lowering of the rotation symmetry. Using a similar method but different pseudopotentials and an exchange correlation potential, Takeda and Shiraishi[44] have examined planar and buckled honeycomb structures of Si. Our results, obtained in a four times larger cell, hence allowing more variational freedom, are in overall agreement with the results in Ref. 44. Moreover, we performed an *ab initio* molecular dynamics calculations on a 2×2 supercell, providing further evidence that the buckled honeycomb structure is stable at 500 K for 250 time steps.

Next we address whether a graphitelike structure of Si (or graphitic Si) can form. Our study distinguished chemisorption and physisorption states in the interlayer interaction, in contrast to only the physisorption state in graphite.[45] The chemisorption state corresponding to a smaller lattice parameter $c=6$ Å is energetically more favorable, namely the binding is 5.1 eV, which is 0.4 eV smaller than that of the bulk Si. We note, however, that lattice parameters and binding energies depend on the approximation of exchange-correlation potential.[46,47] Present GGA calculations yield relatively larger interlayer distance and require the incorporation of long-range Van der Waals (VdW) interaction. Such an analysis showing that the lattice parameter of graphite calculated by GGA is improved by including the VdW attraction, has been presented elsewhere.[48]

Similar to Si, the honeycomb structures of AlP, GaAs, and GaN are found to be stable also, but less energetic relative to the bulk crystal by 0.8, 1.1, and 0.6 eV per basis, respectively. However, the buckling is not favored in order to hinder the formation of a dipole layer.

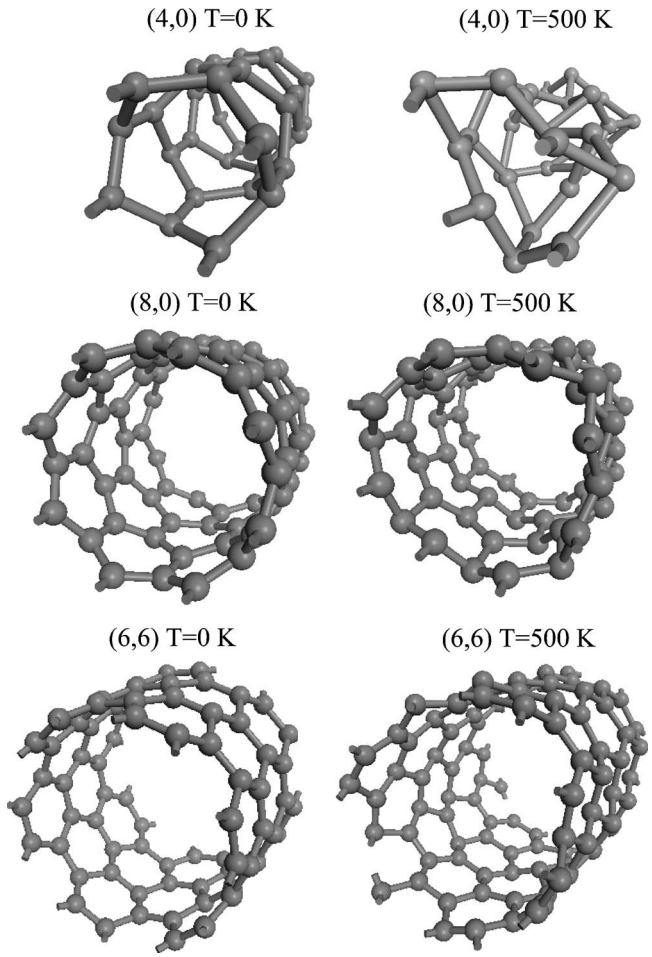

FIG. 2. Structures of (4,0), (8,0), and (6,6) SWSiNTs at $T=0$ and $T=500$ K after 250 time steps. A tubular structure has remained in (6,6) and (8,0) SWSiNT, but the (4,0) structure has clustered.

IV. SINGLE-WALL SILICON NANOTUBES

A. Energetics and stability

Having discussed the stability of buckled Si honeycomb structure (Si-HC), now we present our systematic analysis of $(n,0)$ zigzag and (n,n) armchair SWSiNTs for different n values; namely $n=3-14$ for zigzag and $n=3,6,9$ for armchair structures. The (3,0) zigzag SWSiNT has clustered upon structure relaxation, indicating that it is not stable even at $T=0$ K. While the structure optimization has resulted in regular (4,0) and (5,0) tubular structures, the *ab initio* molecular dynamics (MD) calculations showed that these nanotubes eventually transform into clusters at higher temperatures as shown in Fig. 2. Significant distortions can be easily noticed in (6,0) and also (7,0) SWSiNTs, but tubular character and hexagonal structures on the surface have remained. The (6,0) zigzag tube, which has a radius of $R=3.8$ Å as well as those with larger radii remain stable at temperatures up to 800 K. Barnard and Russo[8] also reported the instability of (3,0) SWSiNT in their first-principles study, but they considered (4,0) and (5,0) SWSiNTs as stable structures, depending on their geometry optimization performed at $T=0$ K. Present results set a limit for fabricating small radius SWSiNTs. The first and second nearest-neighbor interactions between Si atoms become relevant for the stability of small radius nanotubes and causes clusterings, if $R<3.8$ Å. Similar behavior is also obtained for (n,n) armchair SWSiNTs. For example (3,3) SWSiNT is clustered at 800 K in spite of the fact that geometry optimization yields tubular structure at $T=0$ K. On the other hand, the (6,6) tube with a relatively larger radius remained stable at 800 K after 250 time steps. In contrast to (n,n) SWSiNTs, which are found unstable for $n<6$, the (3,3) SWCNT is known to be stable and experimentally fabricated.[49,50] The difference in the chemical behavior of C and Si can be traced to the difference in their π-bonding capabilities. Si tends to utilize all of its three valence p orbitals, resulting in sp^3 hybridization. In contrast, the relatively large promotion energy from C-2s to C-2p orbitals explains how carbon will activate one valence p orbital at a time leading, in turn, to sp, sp^2, sp^3 hybridizations in one-dimensional (1D), 2D, and three-dimensional (3D) structures. This is the explanation why tubular structures of C are more stable than those of Si.[13] Moreover, since the interatomic distance increases significantly in going from C to Si, the π-π overlap decreases accordingly, resulting in much weaker π bonding for Si tubes in comparison with that for carbon tubes.

After the discussion of stability, we next analyze the energetics, namely the behavior of binding energy (E_b) as a

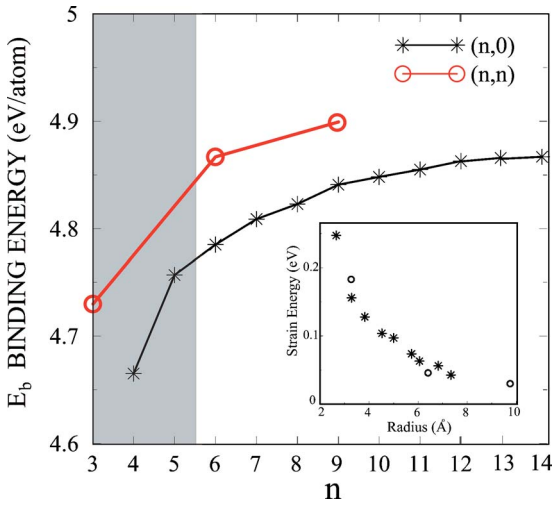

FIG. 3. (Color online) The calculated binding energy per atom for $(n,0)$ zigzag and (n,n) armchair SWSiNTs. The dark region indicates that tubular structures are unstable at finite temperature. The calculated strain energies E_S per atom for $(n,0)$ and (n,n) SWSiNTs are shown in the inset.

function of the radius (or n) of the tube. E_b per atom is calculated using the expression,

$$E_b = \{E_T[\mathrm{SWSiNT}] - N(E_T[\mathrm{Si}])\}/N \quad (1)$$

in terms of the total energy of the optimized SWSiNT having N Si atoms per unit cell, E_T[SWSiNT], and the total energy of N, free Si atom E_T[Si]. It is found that $E_b \sim 4.9$ eV and slightly increases as the radius R (or n) increases for both zigzag and armchair SWSiNTs as displayed in Fig. 3. The energy increase with n is small. According to our results E_bs of (n,n) armchair SWSiNTs are ~ 0.05 eV larger than those of $(n,0)$ zigzag ones because of their relatively larger radius at a given n. Corresponding E_b for SWCNTs is calculated to be 9.1 eV,[51] theoretically.

Finally, the strain energy per atom is calculated relative to the energy of the honeycomb structure,

$$E_S = E_b[\mathrm{SWSiNT}] - (E_b[\mathrm{Si\text{-}HC}]), \quad (2)$$

by subtracting the binding energy (per atom) of optimized honeycomb structure, E_b[Si-HC] from the binding energy of SWSiNT. A slight increase in strain energy is observed as the radius R or n decreases. This is an expected result, since the structure becomes more graphenelike with the increasing radius. Calculated strain energies given by the inset in Fig. 3 are also in agreement with the results obtained by Fagan *et al.*[7] and Barnard and Russo.[8] The calculated value of the strain energy of a zigzag SWSiNT is smaller than the strain energy of a zigzag SWCNT with a comparable radius.[41] In the classical theory of elasticity, the strain (or curvature) energy of a tubular structure is given by the expression $E_S = \alpha/R^2$, where α is a function of Young's modulus and thickness of the tube's wall.[5,52] The results of the present calculations in Fig. 3 gives a fair fit to the expression, α/R^2 with $\alpha \sim 2.07$ eV/Å^2.

B. Mechanical properties

Radial flexibility is a criterion for the stability of tubular structure. SWCNTs are known to be flexible for the deformations in radial directions:[53,54] they can sustain severe radial deformation transforming the circular cross section into an elliptical one with minor (b) and major (a) axes. The radial deformation on a bare tube of radius R is specified in terms of the strain associated with the pressing of the tube along the minor axis, $\epsilon_{yy}=(b-R)/R$ and the strain associated with the expansion of the tube along the perpendicular major axis $\epsilon_{xx}=(a-R)/R$. Theoretical and experimental research has shown that radially deformed tubes relax reversibly to the original circular cross section whenever the external radial force is lifted.[55] Moreover, radial deformation can modify the electronic structure reversibly, which leads to a tunable band gap engineering.[55,56] For example, a semiconducting $(n,0)$ can be metallic under radial deformation. Our results indicate that SWSiNTs display a behavior different than that of SWCNTs. We performed a systematic analysis of radial strain for (8,0) zigzag and (6,6) armchair SWSiNTs. First, these tubes have been deformed by applying $\epsilon_{yy}=-0.1$, -0.2, and -0.3. Then the stress (or constraint) imposing these radial strains has been lifted and the structure has been optimized. Contrary to the situation in carbon nanotubes, up to the applied strain $\epsilon_{yy} \leqslant -0.2$ the SWSiNTs have remained in the deformed state. For example, (8,0) tubes with an initial radial strain of $\epsilon_{yy}=-0.1$ and -0.2 are relaxed to a plastic deformation corresponding to $\epsilon_{yy}=-0.09$ and $\epsilon_{yy}=-0.14$, respectively. Similar results have been obtained for (6,6) armchair SWSiNT with initial radial strain of $\epsilon_{yy}=-0.1$ and -0.2. In contrast, the tubes, which initially strained by $\epsilon_{yy}=-0.25$ and -0.3 have relaxed to a state with negligible residual strain. The total energy of the undeformed SWSiNT E_T^o have been found to be lower (more energetic) than the total energy $E_T^r(\epsilon_{yy})$ of tubes which were relaxed upon radial deformation $-0.3 \leqslant \epsilon_{yy} \leqslant 0$. However, the energy difference $\Delta E = E_T^r(\epsilon_{yy}) - E_T^o > 0$ is very small. The weakness of π bonds of Si as compared to carbon nanotubes is possibly a reason why the restoring forces are not strong enough to derive the deformed state to relax back to the original undeformed state. Once the applied radial deformation gets significant $(|\epsilon_{yy}| > 0.2)$ the restoring forces become strong enough to derive the relaxation towards circular cross section. On the other hand, after a severe radial strain that causes a significant coupling between opposite internal surfaces, the deformed state may be more energetic [i.e., $E_T^r(\epsilon_{yy}) < E_T^o$] or it may relax to different structures such as clusters. This situation constitutes an important difference between Si and C single-wall nanotubes.

The axial strength of SWSiNT, or the elastic stiffness along tube axis, is defined as the second derivative of the strain energy per atom with respect to the axial strain ϵ_{zz}, namely $\kappa = d^2E_T/d\epsilon_{zz}^2$. The elastic stiffness of the (8,0) SWSiNT along its axis is calculated to be 23 eV. This value is significant, but smaller than that of SWCNT which is calculated to be 52–60 eV.[57]

C. Electronic structure

A systematic analysis of the electronic structure indicates that metallic zigzag SWSiNTs $6 \leqslant n \leqslant 11$ have three bands

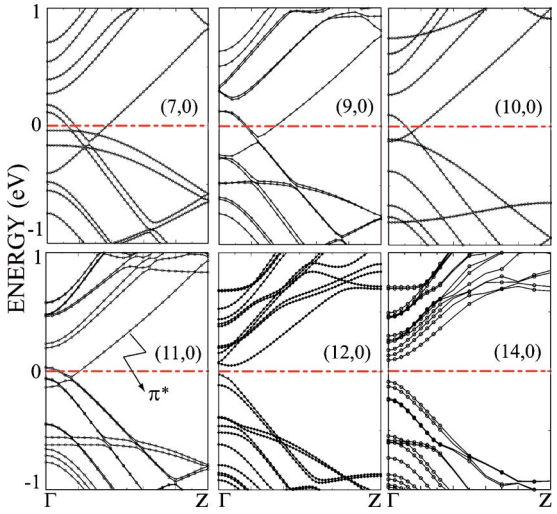

FIG. 4. (Color online) The energy bands calculated for (7,0), (9,0), (10,0), (11,0), (12,0), and (14,0) SWSiNTs using GGA. The lowest conduction band, or singlet π^* band, is indicated. The zeros of energy are set at the Fermi level.

crossing the Fermi level, but a band gap between the valence and conduction bands opens when $n \geqslant 12$. A similar effect has been obtained for zigzag SWCNTs when $n \geqslant 7$.[5,41] This metal-semiconductor transition was attributed to the energy shift of the singlet π^* band which is normally empty, but becomes filled due to increased σ^*-π^* hybridization at a small radius.[41,58] In the present case it appears that σ^*-π^* hybridization becomes significant at a relatively larger radius. The conductance of all these infinite, perfect tubes ($6 \leqslant n \leqslant 11$) is predicted to be equal to $3G_o$ ($G_o = 2e^2/\hbar$). A similar metallic behavior is also obtained for armchair types, namely for (6,6) and (9,9) SWSiNTs. The conductance of ideal infinite (n,n) tubes is $2G_o$, but not $3G_o$, as in metallic $(n,0)$ zigzag tubes. Figure 4 presents the systematic analysis of $(n,0)$ tubes for $7 \leqslant n \leqslant 14$ and clearly shows how the singlet π^* band gradually raises as R increases.

Based on LDA calculations, Fagan *et al.*[6,7] also found (6,6) and (6,0) SWSiNTs metallic, but they predicted (10,0) and (12,0) zigzag nanotubes are semiconductors with a small band gap of 0.1 eV. The disagreement between the present one and those of Fagan *et al.*[6,7] may be due to the differences in pseudopotentials and in the approximation of exchange correlation potential. Note that the transition of $(n,0)$ SWSiNTs from the metallic to the semiconducting state through the gap opening may occur at n, which is smaller than predicted by the present study as well as by Fagan *et al.*,[6,7] if self-energy corrections are taken into account by the *GW* method.[37] Electronic structure analysis performed for the tubes under strain both radially and axially showed that the metallic character is not altered but the position of the Fermi level is slightly changed due to deformation. The modification of the electronic structure with chirality may offer the possibility of fabrication of nanodevices using SWSiNT junctions. On the other hand, SWSiNTs can be used as metallic interconnects, since their conductance is not severely affected by deformation.

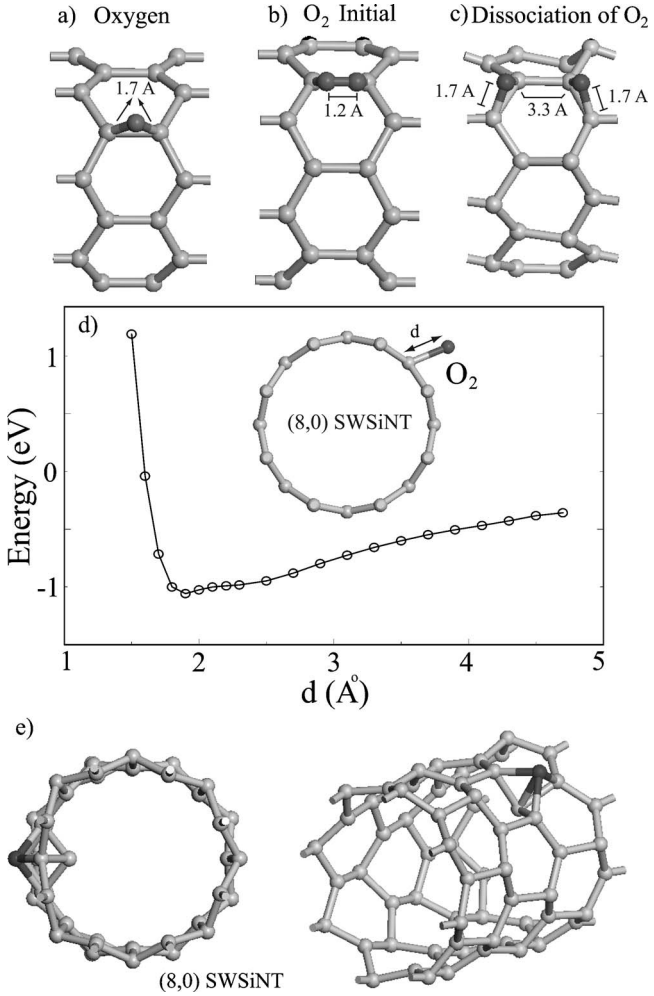

FIG. 5. (a) The optimized geometry of an O atom adsorbed over the axial site of (8,0) SWSiNT. (b) Initial adsorption geometry of O_2 over the axial site. (c) Dissociation of O_2 after relaxation and formation of Si–O–Si bridge bands over the adjacent zigzag Si–Si bonds. (d) Variation of interaction energy as a function of the distance d of an O_2 molecule from the parallel axial Si–Si band. (e) Optimized geometry of a single Si atom adsorbed on the top site (indicated by a dark ball).

D. Interaction of SWSiNT with atoms and molecules

The interaction of Si nanotubes with an oxygen atom and an oxygen molecule is extremely important for technological applications. The adsorption of an oxygen atom is studied by placing it initially above a Si–Si bond parallel to the axis of a (8,0) SWSiNT. The optimized structure shown in Fig. 5(a) has a very strong chemical bonding between O and SWSiNT with $E_b = 8.1$ eV and the nearest Si–O distance 1.7 Å. The resulting geometry showed that SWSiNT is slightly distorted upon O adsorption.

The interaction between O_2 and SWSiNT has been revealed by calculating the binding energy as a function of the separation d from the axial Si–Si bond of the tube as shown in Fig. 5(b). The O_2 molecule is kept unrelaxed and taken parallel to the Si–Si bond. The calculated energy versus distance curve $E(d)$ in Fig. 5(d) shows that O_2 can be attracted to the tube, but there is no physisorption state as in O_2

+SWCNT.[48] The minimum of $E(d)$ occurs at 1.9 Å. Upon relaxation of the tube and O_2 near this minimum, the molecule has been dissociated to form two Si–O–Si bridge bonds over the zigzag Si–Si bonds, and concomitantly SWSiNT has been distorted locally as illustrated in Fig. 5(c). The distances between nearest Si–O and O–O are 1.7 and 3.3 Å, respectively. We repeated the structure relaxation by initially placing O_2 at a larger distance $d=2.5$ Å from the surface of the tube and we obtained the same dissociated state. Our results indicate that there will be a strong interaction between the Si nanotube and the oxygen molecule in open air applications.

The SWSiNT surface is found to be reactive against Si, H, and Au atoms. The Si atom attached to the top site is bound by $E_b \sim 5$ eV. One Si atom of the tube is plunged inside the tube and a small cluster is formed at the surface [see Fig. 5(e)]. The chemisorption energy of H and Au atoms is strong and found to be 4.4 eV and 3.4 eV, respectively.

V. STABILIZATION OF SILICON NANOTUBES BY TRANSITION METAL ATOM DOPING

Recently, Singh *et al.*[15] showed that Si-cluster structures and Si-tubular structures formed by top-to-top stacking of Si hexagons can be stabilized by the implementation of TM atoms inside these structures. Those structures are not only stabilized, but also acquired magnetic properties. Earlier, TM atoms are shown to form rather strong bonds with the carbon atoms on the surface of SWCNTs.[51] Motivated by the work of Singh *et al.*,[15] we investigated whether (3,0) SWSiNT can be stabilized in the same manner. The (3,0) tube has radius $R \sim 2.4$ Å in which interaction between the atoms located at the opposite walls of the tube as well as excess strain on the Si–Si bonds are the prime causes of structural instability even at $T=0$ K. On the other hand, the radius of (3,0) is comparable to the sum of the ionic radii of V and Si, i.e., $R_V+R_{Si}=2.27$ Å, and hence V atoms can easily be accommodated inside the tube. We considered a (3,0) SWSiNT, which has V atoms implemented inside and periodically arranged along the tube axis. Because of the supercell geometry used in the calculations both linear chains (LC) of V atoms (V-LC) and (3,0) tube have a common lattice parameter (see Fig. 6). The optimized structure which that consists of planar hexagons is stacked with V-LC passing through its center, and has been found to be stable. The energy of the V-stabilized structures is lowered by 12.9 eV relative to the energies of the V-LC and the Si tube without V-LC in it but they have the same atomic structures as Si tube with V-LC. Spin-relaxed calculations resulted in zero magnetic moment $\mu=0$. The *p-d* hybridization between Si and V atomic orbitals is the cause of stability and lowering the total energy.

The radius of the unrelaxed (3,3) SWSiNT of 3.7 Å is too large and may not be suitable for its stabilization through the implementation of an atomic chain. Perhaps it may be better suited to accommodate a small clusters of atoms. We considered the possibility whether the (3,3) SWSiNT is stabilized by TM atoms adsorbed on the external surface of the tube. To this end, we studied Ti and Cr atoms adsorbed on the hollow sites (i.e., above the hexagons formed by Si atoms).

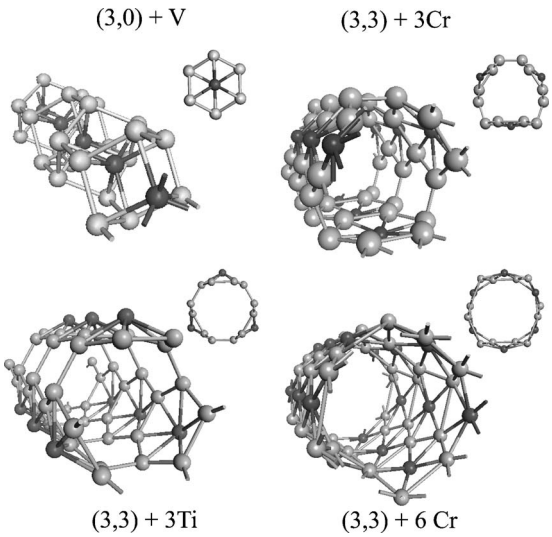

FIG. 6. Perspective and top (cross section) view of the fully relaxed V doped (3,0), Ti-doped, and Cr-doped (3,3) SWSiNTs. Our results revealed that small radius SWSiNTs can be stabilized by a doping transition metal element.

As shown in Fig. 6, we examined three different (3,3) +TM structures: namely, 3 Ti-LC, 3 Cr-LC, and 6 Cr-LC are adsorbed on the (3,3) SWSiNT surface. Spin-relaxed GGA calculations are carried out to optimize the geometric structure. The external absorption 3 Ti-LC [or three Ti atoms per unit cell of (3,3) tube] prevented the tube from collapsing into a cluster, but the circular cross section changed to a polygonal one. The ground state has been predicted to be nonmagnetic with $\mu=0$. The external adsorption of 3 Cr-LC also resulted in a polygonal cross section, but a ferromagnetic ground state with the net magnetic moment $\mu=9.7\mu_B$ (Bohr magneton). The circular cross section is maintained by the adsorption of 6 Cr-LC. This latter structure has also ferromagnetic ground state with $\mu=17.2\mu_B$.

Calculated energy band structures of (3,0)+V, (3,3) +Ti, (3,3)+3 Cr, and (3,3)+6 Cr are presented in Fig. 7. The (3,0)+V structure is a metal. Six bands crossing the Fermi level yield quantum ballistic conductance of $G=6G_0$. The partial density of states indicates that V-3*d* and Si-3*p* orbital character dominate the states at the Fermi level. The (3,3)+3 Ti structure is a semiconductor with a very narrow band gap. In the case of (3,3)+3 Cr and (3,3)+6 Cr several majority (spin-up $\uparrow$) and minority (spin-down $\downarrow$) bands are crossing the Fermi level. Hence both structures are metals with finite density of majority $D(E=E_F,\uparrow)$ and minority $D(E=E_F,\downarrow)$ spin states at E_F. However, $D(E=E_F,\uparrow) - D(E=E_F,\downarrow)$ is significant. These properties, which also depend on the decoration of the tubes, can be used in nanospintronic device applications. Recently Dumitrica *et al.*[10] have investigated the stabilization (3,0) zigzag and (2,2) armchair SWSiNTs by various atoms (Zr, Sc, Ti, Cr, Fe, Ni, Be, and Co) axially placed inside the tube. However, they consider neither the magnetic ground state due to specific TM atoms nor the stabilization of tubes that have a relatively larger radius.

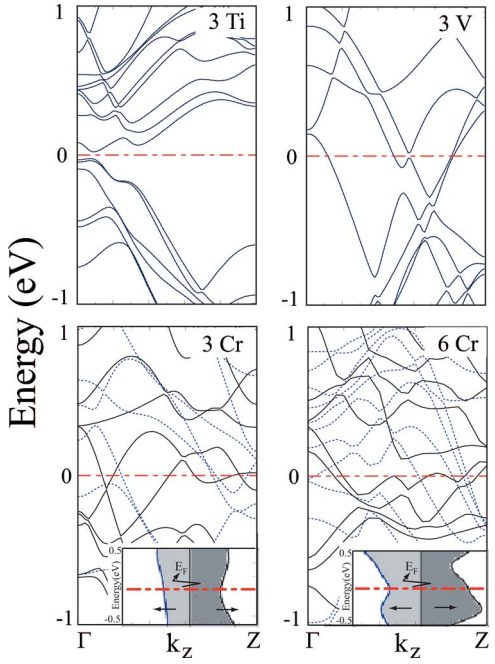

FIG. 7. (Color online) The energy band structures of (3,0)+V, (3,3)+3 Ti, (3,3)+3 Cr, and (3,3)+6 Cr calculated by using the self-consistent-field spin-polarized GGA method. Solid lines and dotted lines are for majority and minority states, respectively. The inset shows the density of majority (dark) and minority (light) spin states at the Fermi level of (3,3)+3 Cr and (3,3)+6 Cr structures.

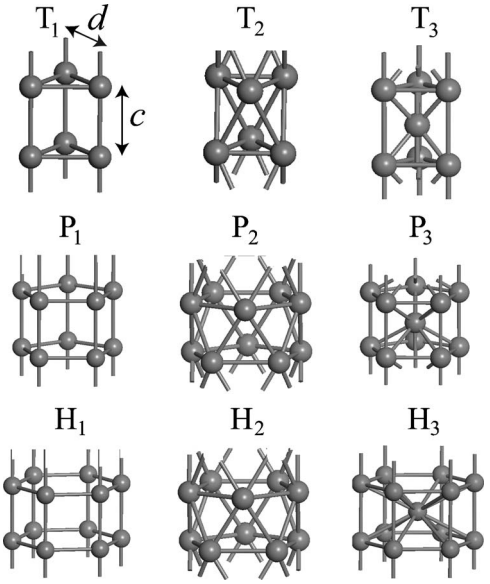

FIG. 8. Some tubular structures of Si. The tubes are formed by the stacking of Si polygons; the labels T, P, and H stand for triangular, pentagonal, and hexagonal configurations, respectively. T_1, P_1, and H_1 tubes have top-to-top arrangement of layers. In T_2, P_2, and H_2 the layers are staggered. T_3, P_3, and H_3 structures have extra atoms centered in between the layers.

VI. OTHER TUBULAR STRUCTURES OF SILICON

We now consider different tubular structures which are formed by the stacking of atomic polygons as presented in Fig. 8. Three tubular structures given in the first row, i.e., T_1, T_2, T_3, are made of triangles of silicon atoms, which are stacked along the axis of the tube. In T_1, triangles are identical and placed in a top-to-top (or eclipsed) position; in T_2 the triangles are staggered; a T_3 structure is constructed by the insertion of a Si linear chain (Si-LC) into the T_1 structure as such that the chain atoms are centered in between the layers. The same convention is followed in labeling the tubular silicon nanowires with pentagonal (P_1,P_2,P_3) and hexagonal (H_1,H_2,H_3) cross sections.

Starting with those geometries, structural optimizations in large supercells yielded T_2, T_3, and H_3 as unstable, which deformed into clusters. The structural parameters, the binding energies, and equilibrium conductance values of stable tubular structures are summarized in Table I. All the stable silicon tubes have comparable binding energy values, with the P_1 structure being slightly more favorable energetically. Also within each set of tubular structures the top-to-top arrangement provides the highest cohesive energy. In Fig. 9 the energy band structure and equilibrium conductance plots of T_1, P_1, and H_1 structures are presented. All of them are found metallic with calculated ideal conductance values of $6G_0$, $10G_0$, and $6G_0$, respectively. A common feature noticed in the energy band structures of T_1, P_1, and H_1 tubes is that there are almost filled bands available in close vicinity of the Fermi levels, which may lead to drastic conductance variations due to small structural perturbations in the tubes or small bias voltage.

Earlier, the pentagonal nanowires of Si and also those of several metals such as Na, Al, Cu, Pb, Au, Fe, Ni, and Xe were investigated by Sen *et al.*[59] using similar calculation methods. The results for a specific structure, P_3, which is common in both studies, is in agreement. The stability of the P_3 is further strengthened by the finite-temperature *ab initio* molecular dynamics calculation carried out in the present study. Recently, Bai *et al.*[60] have studied the stability of infinite and finite S_1 (top-to-top square), P_1 and H_1 structures by performing *ab initio* calculations using different methods, including pseudopotential plane waves and classical molecu-

TABLE I. Structural and conductance properties of silicon tubular structures that are found stable. E_b is the binding energy per atom, c is the unit cell length of the periodic structure, and d is the in-plane bond lengths of the polygonal atomic layers. Equilibrium conductance values are given by G in units of conductance quantum, $G_o=2e^2/h$.

Structure	E_b (eV)	c (Å)	d (Å)	G $(2e^2/h)$
T_1	4.62	2.37	2.38	6
T_2				
T_3				
P_1	4.79	2.37	2.37	10
P_2	4.68	2.70	2.46	10
P_3	4.66	4.10	2.58	6
H_1	4.77	2.29	2.37	6
H_2	4.74	2.52	2.42	9
H_3				

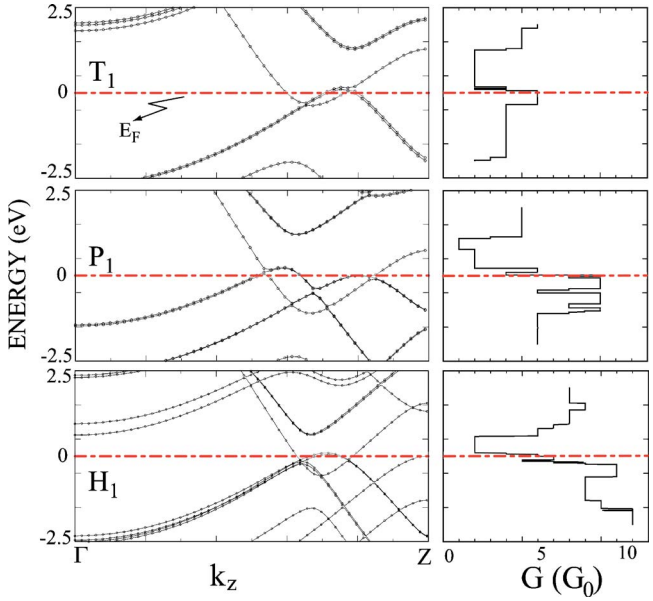

FIG. 9. (Color online) Energy band structure of Si tubular structures formed by the top-to-top stacking of triangular (T_1), pentagonal (P_1), and hexagonal (H_1) polygons. In the right panels the corresponding equilibrium conductance in $G_o=2e^2/h$ curves are plotted. The Fermi levels are set to zero.

lar dynamics calculations at 2000 K. Their stability analysis for P_1 and H_1 are in agreement with present results. In addition to P_1 and H_1, the present study deals with T_1 and also staggered ones.

VII. SINGLE-WALL NANOTUBES OF III-V COMPOUNDS

Motivated by interesting properties of SW(BN)NT and opto-electronic and field emitting properties of GaN and AlN tubular forms,[21,25] we choose (8,0) AlP, GaAs, and GaN single-wall nanotubes as prototypes to investigate the stability and electronic properties of III-V compound nanotubes. Even if the single-wall nanotubes of these compounds have not been sythesized yet, the predictions of the present work are essential for further efforts to achieve. The initial bond lengths are chosen as the distance between nearest cation and anion atoms in bulk structure. After relaxation of all atomic positions, as well as lattice constant c, the tubular structures remained stable. The *ab initio* MD calculations also showed that SW(AlP)NT remained stable at room temperature after 250 time steps. E_b is calculated to be 9.6 eV per AlP basis. The radius of the tube is 5.2 Å. The structure is not a perfect tube but the hexagons on the surface are buckled. The nearest Al–P distance is 2.3 Å, and second nearest-neighbor distance i.e., nearest P–P and Al–Al distances, are 3.9 Å and 3.8 Å, respectively. The energy band and TDOS analysis in Fig. 10 points out that (8,0) SW(AlP)NT is a semiconductor (insulator) with a band gap of 2.0 eV.

Initial tubular structure of (8,0) SW(GaAs)NT is maintained after geometry optimization at $T=0$ K. Similar to SW(AlP)NT, hexagons are buckled. E_b is calculated to be 7.7 eV per GaAs and the radius is 4.8 Å. The nearest Ga–As distance is 2.4 Å, and the nearest Ga–Ga and As–As distances are 3.9 Å and 4.1 Å, respectively. The (8,0) SW(GaAs)NT is also a semiconductor (insulator) with a band gap of 0.9 eV.

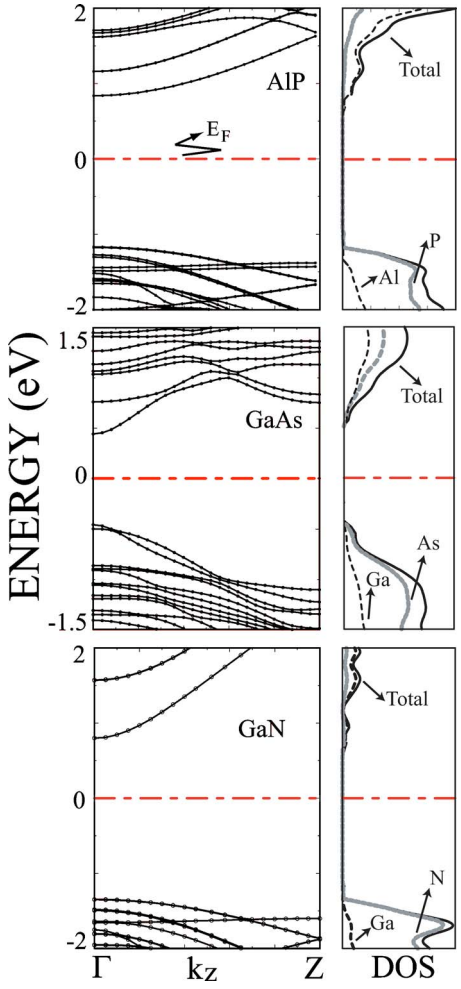

FIG. 10. (Color online) Energy band structures (left panels), TDOS, and partial density of states on atoms (right panels) of (8,0) zigzag SW(AlP)NT, SW(GaAs)NT, and SW(GaN)NT. Anion (Al, Ga) and cation (P, As, N) contributions to TDOS are shown by dashed and light continuous lines. Zero of the energy is set at the Fermi level.

We place a special emphasis on GaN nanotubes,[20,61] which are successfully synthesized by an epitaxial casting method where ZnO nanowires are initially used as templates. GaN nanotubes produced this way have a diameter of 300 Å and a minimum wall thickness of 50 Å. They are semiconducting and hence they would be a possible candidate for opto-electronic applications. Whether a single-wall GaN tube of smaller diameter ($2R\sim 10$ Å) can be stable and can exhibit technologically interesting electronic properties is important to know. We again took (8,0) SW(GaN)NT as a prototype for the sake of consistency. Stable tubular geometry is obtained by both geometry optimization at $T=0$ K and *ab initio* MD analysis at $T=800$ K. Upon relaxation, atoms on the surface are buckled. E_b is calculated to be 11.5 eV per GaN and the radius is 4.1 Å. The nearest Ga–N distance is 1.8 Å, and the nearest Ga–Ga and N–N distances are 3.1 Å and 3.2 Å, respectively. We found that the (8,0)

TABLE II. Calculated binding energies E_b and bond distances d in Å of various structures of Si, AlP, GaAs, and GaN. B is a 3D bulk crystal, H is a 2D honeycomb structure, and T is the (8,0) single-wall nanotube structure. The units of binding energy are eV/atom for Si and eV/basis for III-V compounds.

	Si			AlP			GaN			GaAs		
	B	*H*	*T*	*B*	*H*	*T*	*B*	*H*	*T*	*B*	*H*	*T*
E_b (eV)	5.4	4.9	4.8	10.4	9.6	9.6	12.4	11.8	11.5	8.3	7.8	7.7
d (Å)	2.3	2.3	2.3	2.4	2.2	2.3	2.0	1.8	1.8	2.4	2.2	2.4

SW(GaN)NT is a semiconductor (insulator) with a band gap of 2.2 eV. A previous first-principles study performed by Lee *et al.*[23] by using a LDA method predicted the similar band gap for SW(GaN)NT. Here, we examine also whether SW(GaN)NT is radially elastic. To this end we started with the elliptically deformed nanotube under $\epsilon_{yy}=-0.1$ and let it relax in the absence of radial forces. Similar to the Si nanotube, SW(GaN)NT is found to be radially soft.

For the sake of comparison, the binding energy and bond distance of bulk crystals, honeycomb structures, and (8,0) tubular structures of Si, AlP, GaN, and GaAs are presented in Table II. In these structures the covalent or (covalent-ionic) mixed bonds have different orbital combinations. While bulk crystals are tetrahedrally coordinated and have bonds formed by sp^3-hybrid orbitals, in honeycomb and tubular structures bonding through sp^2-hybrid orbitals dominates the cohesion.

VIII. CONCLUSION

In this paper, we analyzed the stability of Si and III-V compound, single-wall nanotubes, and calculated their optimized atomic structure and energy band structure. Si as well as III-V compounds can form a stable 2D honeycomb structure, which is precursor of nanotubes. The energy necessary to roll these honeycomb structures over a cylinder of radius R to make a perfect nanotube is small, however, as compared to those in carbon nanotubes. We found that Si single-wall nanotubes with small radius are unstable and are clustered either at $T=0$ K or at finite temperatures. For example, while (3,0) is unstable even at $T=0$ K, (4,0) and (5,0) lose their tubular character and tend to form cluster at $T=500$ K. Stable $(n,0)$ zigzag SWSiNTs are metallic for $6\leqslant n\leqslant 11$, but become semiconducting for $n\leqslant 12$. The metallicity of small radius $(n,0)$ tubes is a typical curvature effect and results from the dipping of the singlet π^* band into the valence band at small radius. Stable (n,n) armchair SWSiNTs $(n=6,9)$ are metallic. Our study on radially deformed (8,0) and (6,6) SWSiNTs demonstrated that these nanotubes are radially "soft," and hence are devoid of the strong restoring force that maintains radial elasticity. The radial softness of Si tubes is a behavior which distinguishes them from carbon nanotubes. In contrast to that axial stiffness the Si nanotube has been found to be high. We predicted that oxygen molecules adsorbed on the Si–Si bonds dissociates. A strong interaction between O/O_2 and SWSiNT appears to be serious in future processes involving Si tubes. Adatoms like Si, Au, and H can also form strong chemisorption bonds with the atoms on the surface of SWSiNT. We showed that unstable, small radius SWSiNTs can be stabilized through the implementation or external adsorption of $3d$ transition metal atoms. In particular, the decoration of the tube surface by the external adsorption of transition metal atoms can lead to magnetic properties, which may find potential technological applications. Small radius tubular structures different than those based on the honeycomb structure have been identified. Finally, we found III-V compound (8,0) nanotubes (AlP, GaAs, and GaN) stable at least at room temperature and they are semiconductors with band gaps ranging from 0.9 eV to 2.2 eV. In contrast to small radius metallic Si nanotubes, (8,0) compound nanotubes are semiconductors. The band gap increases with a decreasing row number of elements. Even though not all the structures treated in this study have been realized experimentally, the predictions obtained from the present first-principles calculations are expected to be essential for further research in this field.

ACKNOWLEDGMENTS

Part of the computations has been carried out at ULAKBIM Computer Center. S.C. acknowledges partial financial support from Academy of Science of Turkey.

*Corresponding author.
Electronic address: ciraci@fen.bilkent.edu.tr

[1] S. Iijima, Nature (London) **354**, 56 (1991); S. Iijima, T. Ichihashi, and Y. Ando, Nature (London) **356**, 776 (1992).

[2] M. S. Dresselhaus, G. Dresselhaus, and P. C. Eklund, *Science of Fullerenes and Carbon Nanotubes* (Academic, San Diego, CA, 1996).

[3] R. Saito, G. Dresselhaus, and M. S. Dresselhaus, *Physical Properties of CarbonNanotubes* (Imperial College, London, 1998).

[4] J. W. Mintmire, B. I. Dunlap, and C. T. White, Phys. Rev. Lett. **68**, 631 (1992).

[5] For the most recent review on the functionalization and the electronic properties of single-wall carbon nanotubes and for additional references, see, for example, S. Ciraci, T. Yildirim, S. Dag, O. Gülseren, and R. T. Senger, J. Phys.: Condens. Matter **16**, R901 (2004).

[6] S. B. Fagan, R. J. Baierle, R. Mota, A. J. R. da Silva, and A. Fazzio, Phys. Rev. B **61**, 9994 (1999).

[7] S. B. Fagan, R. Mota, R. J. Baierle, G. Paiva, A. J. R. da Silva, and A. Fazzio, J. Mol. Struct.: THEOCHEM **539**, 101 (2000).

[8] A. S. Barnard and S. P. Russo, J. Phys. Chem. B **107**, 7577 (2003).
[9] V. V. Ivanovskaya, A. A. Sofronov, and A. L. Ivanosvkii, Phys. Lett. A **297**, 436 (2002).
[10] T. Dumitrica, M. Hua, and B. I. Yakobson, Phys. Rev. B **70**, 241303(R) (2004).
[11] O. Ponomarenko, M. W. Radny, and P. V. Smith, Surf. Sci. **562**, 257 (2004).
[12] M. Zhang, Y. H. Kan, Q. J. Zang, Z. M. Su, and R. S. Wang, Chem. Phys. Lett. **379**, 81 (2003).
[13] R. Q. Zhang, S. T. Lee, C. K. Law, W. K. Li, and B. K. Teo, Chem. Phys. Lett. **364**, 251 (2002).
[14] G. Seifert, Th. Köhler, K. H. Urbassek, E. Hernàndez, and Th. Frauenheim, Phys. Rev. B **63**, 193409 (2001).
[15] A. K. Singh, T. M. Briere, V. Kumar, and Y. Kawazoe, Phys. Rev. Lett. **91**, 146802 (2003).
[16] B. Marsen and K. Sattler, Phys. Rev. B **60**, 11593 (1999).
[17] J. Sha, J. Niu, X. Ma, J. Xu, X. Zhang, Q. Yang, and D. Yang, Adv. Mater. (Weinheim, Ger.) **14**, 1219 (2002); J. Niu, J. Sha, and D. Yang, Physica E (Amsterdam) **23**, 131 (2004).
[18] A. Loiseau, F. Willaime, N. Demoncy, G. Hug, and H. Pascard, Phys. Rev. Lett. **76**, 4737 (1996); J. S. Lauret, R. Arenal, F. Ducastelle, A. Loiseau, M. Cau, B. Attal-Tretout, E. Rosencher, and L. Goux-Capes, Phys. Rev. Lett. **94**, 037405 (2005).
[19] Z. Liliental-Weber, Y. Chen, S. Ruvimov, and J. Washburn, Phys. Rev. Lett. **79**, 2835 (1997).
[20] J. Goldberger, R. He, Y. Zhang, S. Lee, H. Yan, H. Choi, and P. Yang, Nature (London) **422**, 599 (2003).
[21] V. N. Tondare, C. Balasubramanian, S. Shende, D. S. Joag, V. P. Godbale, and S. V. Bhoraskar, Appl. Phys. Lett. **80**, 4813 (2002).
[22] A. Rubio, J. L. Corkill, and M. L. Cohen, Phys. Rev. B **49**, R5081 (1994).
[23] S. M. Lee, Y. H. Lee, Y. G. Hwang, J. Elsner, D. Porezag, and T. Frauenheim, Phys. Rev. B **60**, 7788 (1999).
[24] M. Cote, M. L. Cohen, and D. J. Chadi, Phys. Rev. B **58**, R4277 (1998).
[25] M. Zhao, Y. Xia, D. Zhang, and L. Mei, Phys. Rev. B **68**, 235415 (2003).
[26] L. Rapoport, Y. Bilik, Y. Feldman, M. Homyonfer, S. R. Cohen, and R. Tenne, Nature (London) **387**, 791 (1997).
[27] Y. Feldman, E. Wasserman, D. J. Srolovitz, and R. Tenne, Science **267**, 222 (1995).
[28] R. Tenne, L. Margulis, M. Genut, and G. Hodes, Nature (London) **360**, 444 (1992).
[29] Y. R. Hacohen, E. Grunbaum, R. Tenne, J. Sloand, and J. L. Hutchinson, Nature (London) **395**, 336 (1998).
[30] M. C. Payne, M. P. Teter, D. C. Allen, T. A. Arias, and J. D. Joannopoulos, Rev. Mod. Phys. **64**, 1045 (1992).
[31] Numerical computations have been carried out by using VASP software: G. Kresse and J. Hafner, Phys. Rev. B **47**, R558 (1993); G. Kresse and J. Furthmuller, Phys. Rev. B **54**, 11169 (1996).
[32] W. Kohn and L. J. Sham, Phys. Rev. **140**, A1133 (1965); P. Hohenberg and W. Kohn, Phys. Rev. **136**, B864 (1964).
[33] D. Vanderbilt, Phys. Rev. B **41**, R7892 (1990).
[34] J. P. Perdew, J. A. Chevary, S. H. Vosko, K. A. Jackson, M. R. Pederson, D. J. Singh, and C. Fiolhais, Phys. Rev. B **46**, 6671 (1992).
[35] M. Methfessel and A. T. Paxton, Phys. Rev. B **40**, 3616 (1989).
[36] H. J. Monkhorst and J. D. Pack, Phys. Rev. B **13**, 5188 (1976).
[37] For an extensive discussion of the *GW* method: F. Aryasetiawan and O. Gunnarsson, Rep. Prog. Phys. **61**, 237 (1998).
[38] T. Miyake and S. Saito, Phys. Rev. B **68**, 155424 (2003).
[39] C. D. Spataru, S. Ismail-Beigi, L. X. Benedict, and S. G. Louie, Phys. Rev. Lett. **92**, 077402 (2004); Appl. Phys. A **78**, 1129 (2004).
[40] Y. Ouyang, J. Huang, C. L. Cheung, and C. M. Lieber, Science **292**, 702 (2001).
[41] O. Gülseren, T. Yildirim, and S. Ciraci, Phys. Rev. B **65**, 153405 (2002).
[42] S. Nosé, Mol. Phys. **52**, 255–268 (1984).
[43] U. Röthlisberger, W. Andreoni, and M. Parrinello, Phys. Rev. Lett. **72**, 665 (1994).
[44] K. Takeda and K. Shiraishi, Phys. Rev. B **50**, 14916 (1994).
[45] The same problem, as well as the energetics of graphite by itself have been treated by Y. C. Wang, K. Scheerschmidt, and U. Gosele, Phys. Rev. B **61**, 12864 (2000). In this paper, the interaction energies of physisorption and chemisorption states are equal for a fixed lattice parameter $a=3.86$ Å. However, the results indicate that a should differ by going from physisorption to chemisorption. We also found that planar Si layers are buckled and the energy difference between α and β configuration is only 100 meV.
[46] J. C. Charlier, X. Gronze, and J. P. Michenoud, Europhys. Lett. **28**, 4040 (1994).
[47] W. Kohn, Y. Meir, and D. E. Makarov, Phys. Rev. Lett. **80**, 4153 (1998).
[48] S. Dag, O. Gülseren, T. Yildirim, and S. Ciraci, Phys. Rev. B **67**, 165424 (2003).
[49] Z. K. Tang *et al.*, Science **292**, 2462 (2001).
[50] N. Wang, Z. K. Tang, G. D. Li, and J. S. Chen, Nature (London) **408**, 50 (2000).
[51] E. Durgun, S. Dag, V. K. Bagci, O. Gülseren, T. Yildirim, and S. Ciraci, Phys. Rev. B **67**, 201401(R) (2003); E. Durgun, S. Dag, S. Ciraci, O. Gülseren, J. Phys. Chem. B **108**(2), 575 (2004).
[52] D. H. Robertson, D. W. Brenner, and J. W. Mintmire, Phys. Rev. B **45**, R12592 (1992); G. G. Tibbets, J. Cryst. Growth **66**, 632 (1984); K. N. Kudin, G. E. Scuseria, and B. I. Yakobson, Phys. Rev. B **64**, 235406 (2001).
[53] T. W. Tombler, C. W. Zhou, L. Alexseyev, J. Kong, H. J. Dai, L. Lei, C. S. Jayanthi, M. J. Tang, and S. Y. Wu, Nature (London) **405**, 769 (2000).
[54] P. Zhang, P. E. Lammert, and V. H. Crespi, Phys. Rev. Lett. **81**, 5346 (1998).
[55] O. Gülseren, T. Yildirim, S. Ciraci, and C. Kilic, Phys. Rev. B **65**, 155410 (2002).
[56] C. Kilic, S. Ciraci, O. Gülseren, and T. Yildirim, Phys. Rev. B **62**, R16345 (2000).
[57] D. Sanchez-Portal, E. Artacho, J. M. Soler, A. Rubio, and P. Ordejon, Phys. Rev. B **59**, 12678 (1999).
[58] X. Blase, L. X. Benedict, E. L. Shirley, and S. G. Louie, Phys. Rev. Lett. **72**, 1878 (1994).
[59] P. Sen, O. Gulseren, T. Yildirim, I. P. Batra, and S. Ciraci, Phys. Rev. B **65**, 235433 (2002).
[60] J. Bai, X. C. Zang, H. Tanaka, and J. Y. Zang, Proc. Natl. Acad. Sci. U.S.A. **101**, 2664 (2004).
[61] M. W. Lee, H. C. Hsueh, H.-M. Lin, and C.-C. Chen, Phys. Rev. B **67**, 161309(R) (2003).